J. Cell. Mol. Med. Vol 15, No 4, 2011 pp. 837-849

Molecular MRI assessment of vascular endothelial growth factor receptor-2 in rat C6 gliomas

Ting He [a, b], Nataliya Smith [a], Debra Saunders [a], Sabrina Doblas [a], Yasuko Watanabe [a], Jessica Hoyle [a], Robert Silasi-Mansat [c], Florea Lupu [c], Megan Lerner [d], Daniel J. Brackett [d], Rheal A. Towner [a, b, *]

[a] *Advanced Magnetic Resonance Center, Oklahoma Medical Research Foundation, Oklahoma City, OK, USA*
[b] *The Oklahoma Center for Neurosciences, The University of Oklahoma Health Sciences Center, Oklahoma City, OK, USA*
[c] *Cardiovascular Biology, Oklahoma Medical Research Foundation, Oklahoma City, OK, USA*
[d] *O'Donoghue Research Institute, The University of Oklahoma Health Sciences Center, Oklahoma City, OK, USA*

Received: December 8, 2009; Accepted: March 19, 2010

Abstract

Angiogenesis is essential to tumour progression and a precise evaluation of angiogenesis is important for tumour early diagnosis and treatment. The quantitative and dynamic *in vivo* assessment of tumour angiogenesis can be achieved by molecular magnetic resonance imaging (mMRI). Vascular endothelial growth factor (VEGF) and VEGF receptors (VEGFRs) are the main regulatory systems in angiogenesis and have been used as hot targets for radionuclide-based molecular imaging. However, little research has been accomplished in targeting VEGF/VEGFRs by mMRI. In our study, we aimed to assess the expression of VEGFR2 in C6 gliomas by using a specific molecular probe with mMRI. The differential uptake of the probe conjugated to anti-VEGFR2 monoclonal antibody, shown by varied increases in T_1 signal intensity during a 2 hr period, demonstrated the heterogeneous expression of VEGFR2 in different tumour regions. Microscopic fluorescence imaging, obtained for the biotin group in the probe with streptavidin-Cy3, along with staining for cellular VEGFR2 levels, laminin and CD45, confirmed the differential distribution of the probe which targeted VEGFR2 on endothelial cells. The angiogenesis process was also assessed using magnetic resonance angiography, which quantified tumour blood volume and provided a macroscopic view and a dynamic change of the correlation between tumour vasculature and VEGFR2 expression. Together these results suggest mMRI can be very useful in assessing and characterizing the expression of specific angiogenic markers *in vivo* and help evaluate angiogenesis associated with tumour progression.

Keywords: VEGFR2 • molecular MRI (mMRI) • biotin-Gd-DTPA-albumin-anti-VEGFR2 probe • angiogenesis • C6 rat glioma

Introduction

Angiogenesis is of critical importance to tumour development and metastasis. When a tumour grows to a certain volume, new blood vessels sprouting from established vessels are formed to supply the tumour in excess nutrients and remove waste [1]. It has been established that the degree of neovascularization is well correlated with tumour malignancy and is thus one of the key criteria for grading tumours in patients [2, 3]. The angiogenic switch is well controlled and triggered by pro-angiogenic factors. Vascular endothelial growth factor (VEGF) is the most potent and specific mitogen for stimulating cascades of angiogenesis in endothelial cells [4]. The tyrosine kinase receptor VEGFR2 is the main receptor that is responsible for mediating the promotion of angiogenesis both in embryogenesis and adulthood pathological conditions [5, 6]. The fact that tumour vasculature exhibits an up-regulated VEGFR2 expression makes VEGFR2 a hot potential target for anti-angiogenic therapy in recent years [7, 8]. VEGFR2 is mainly expressed on the surface of activated non-quiescent endothelial cells [9], and this characteristic makes it a suitable target for molecular magnetic resonance imaging (mMRI).

The outcome of human malignant gliomas (especially glioblastoma multiforme, GBM) is very poor, despite traditional clinical therapies. GBM, the most common type of glioma, is characterized by a high-degree of vascularization [10]. This has brought a demand for early and accurate means of defining the

*Correspondence to: Dr. Rheal A. TOWNER,
Director, Advanced Magnetic Resonance Center,
Oklahoma Medical Research Foundation, 825 NE 13th Street,
Oklahoma City, OK 73104, USA.
Tel.: (405) 271–7383
Fax: (405) 271-7254
E-mail: Rheal-Towner@omrf.org

doi:10.1111/j.1582-4934.2010.01091.x

degree of angiogenesis and evaluating the angiogenesis response to anti-angiogenic therapy. Magnetic resonance angiography (MRA) is a non-invasive method to assess both the morphologic alterations of brain vasculature and total cerebral blood volume. mMRI would be ideal for detection of the expression of specific angiogenic markers located on the walls of tumour blood vessels, and thus provide a way to quantify angiogenesis *in vivo*. Several angiogenic markers have been tested with mMRI. MRI of anti-E-selectin monoclonal antibody (mAb) conjugated to iron-oxide nanoparticles was used to assess the binding to human endothelial umbilical vein cells *in vitro* and *in vivo* [11, 12]. Winter *et al*. detected $\alpha_v\beta_3$ integrin overexpression in a rabbit tumour model by using Gadolinium (Gd)-containing nanoparticles coupled to a $\alpha_v\beta_3$ peptidomimetic antagonist [13]. Backer *et al*. demonstrated increased binding to VEGFR2 in xenografted breast tumours as compared to VEGFR2-receptor-blocked mice by using near infrared imaging with VEGF linked to a dendrimer [14]. However, the *in vivo* investigation of molecular imaging targeting VEGFR2 is still lacking.

The goal of this study was to use anti-VEGFR2-mAb linked by albumin-[Gd-diethylene penta-acetic acid (DTPA)]-biotin to detect the angiogenic marker VEGFR2 in a C6 rat glioma model, combined with MRA to assess the new blood vessels (angiogenesis) associated with the tumour. We previously used MRA to detect decreased angiogenesis in a C6 rat glioma model treated with Phenyl-tert-butyl nitrone [15]. We also measured the overexpression of c-Met *in vivo* by using an anti-c-Met mAb conjugated to albumin-(Gd-DTPA)-biotin in C6 rat gliomas, and by using streptavidin-super paramagnetic iron oxide in a hepatocarcinogenesis model [16, 17]. Albumin-(Gd-DTPA) is one of the new-emerging macromolecular contrast media used in dynamic contrast-enhanced MRI, which produces differential enhancement by leaking through the junctions of hyper-permeable endothelial cells in tumour but not in normal tissue [18]. In this study, the probe VEGFR2-albumin-(Gd-DTPA)-biotin successfully targeted extracellular VEGFR2 on angiogenic endothelial cells, and was able to assess the heterogeneous characteristics of VEGFR2 expression associated with angiogenesis during glioma progression. This method may provide valuable information for the evaluation of tumour angiogenesis.

Materials and methods

Intracerebral glioma cell injection

A C6 glioma cell implantation protocol was created by modification of the method described by N. Kobayashi *et al*. [19], and previously published by our group [15]. Briefly, 3-month-old male Fischer 344 rats (250–300 g, Harlan Laboratories, Indianapolis, IN, USA) were anesthetized with 2.5% isoflurane and 0.8 l/min. oxygen, and immobilized on a stereotaxic unit (Stoelting Co., Kiel, WI, USA). The skin of the head was disinfected and incised. A hole was drilled through the skull 2 mm lateral and 2 mm anterior to the bregma, on the right-hand side of the skull. Ten thousand (10^4) C6 cells in 10 μl cell culture media and 1% ultra-low gelling temperature agarose (Sigma-Aldrich, St. Louis, MO, USA) were injected into the cortex at a 3 mm depth from the dura at a rate of 2/min. Bone wax was added into the hole to prevent reflux of the cell suspension. After surgery, rats were fed with a choline-deficient diet to encourage the tumour cell growth [20].

Immunohistochemistry

The brains of rats that had undergone MRA and not administered MRI contrast agents were extracted, fixed by immersion in 10% buffered zinc formalin and embedded in paraffin. The brain sections were immunostained with a mouse mAb anti-VEGFR2 (dilution of 1:200, Santa Cruz Biotech, Inc., Santa Cruz, CA, USA) followed by Rat HRP-Polymer system (Biocare Medical, Concord, CA, USA) for detection and NovaRed (Vector Laboratories, Inc., Burlingame, CA, USA) chromogen for visualization.

Western blots

Brain tissue was weighed and diced into small pieces and then thawed in lysis buffer containing proteases and phosphatase inhibitors. Tissue was disrupted and homogenized at 4°C, incubated on ice for 30 min., and centrifuged (10,000 × *g*, 10 min., 4°C). The supernatant fluid was the total cell lysate. After determining total protein concentrations, electrophoresis of lysates was performed on SDS-PAGE (Bio-Rad, Emeryville, CA, USA), and lysates were transferred to nitrocellulose membranes. Western analysis was performed using antibodies VEGFR2 (anti-VEGFR2 mouse mAb; Santa Cruz Biotech, Inc.). Secondary antibodies were labelled with horseradish peroxidase. The ECL Advance Western Blotting Detection Kit (Amersham Biosci., Piscataway, NJ, USA) was used to detect immunoreactive proteins.

Synthesis of anti-VEGFR2 MRI agent

The contrast agent, biotin-BSA (bovine serum albumin)-Gd-DTPA, was prepared based on the modification of the method developed by Dafni *et al*. [21]. The detailed methodology is referenced as described by Towner *et al*. [16]. Briefly, after biotin-BSA-Gd-DTPA was synthesized, anti-VEGFR2 mAb (Santa Cruz Biotech, Inc.) was conjugated to the albumin moiety through a sulfo-N-hydroxysuccinimide-1-ethyl-3-[3-dimethylaminopropyl]carbodiimido hydrochloride (NHS-EDC) link according to the protocol of Hermanson [22]. The product was lyophilized, stored at 4°C and reconstituted in phosphate buffered saline (PBS) to an appropriate concentration for injections. Each animal was injected with 200 μl anti-VEGFR2-BSA-Gd-DTPA-biotin (VEGFR2 probe) intravenously (i.v.) *via* the tail vein with an amount estimated to be 200 μg anti-VEGFR2 and 100 mg biotin-BSA-Gd-DTPA per injection. The estimated molecular weight of the VEGFR2 probe is estimated to be 232 kD. As a control, normal rat-IgG (obtained from a healthy rat population; Alpha Diagnostic International, San Antonio, TX, USA) conjugated to biotin-BSA-Gd-DTPA (control IgG contrast agent) was synthesized by the same protocol, and injected in a similar fashion, as described above.

MRI, MRA and mMRI

MRI experiments were carried out on a Bruker Biospec 7.0 Tesla/30 cm horizontal-bore magnet small animal imaging system (Bruker Biospin, Ettlingen, Germany). Animals were restrained by using 1–2% isoflurane

and 0.8 l/min. O_2, and placed in a radiofrequency resonator MR probe (72 mm quadrature volume coil) for signal transmission, and a curved rat head surface coil was used for signal reception. T_2-weighted imaging was acquired by using a spin-echo sequence with a repetition time (TR) of 2400 msec. and an echo time (TE) of 64 msec., with 20 transverse slices of 1 mm thickness, and a field of view of 3.5×3.5 cm^2. Tumour volumes were measured using ImageJ (NIH) software.

For mMRI, three rats were used for each of the two groups, which consisted of those administered either a VEGFR2 probe or a non-specific control IgG contrast agent. Tumour volumes were regularly monitored and mMRI data were acquired when the tumour volumes reached approximately >80 mm^3. A variable-TR RARE sequence (rapid acquisition with refocused echoes, with multiple TRs of 200, 400, 800, 1200 and 1600 msec., TE of 15 msec., field of view of 3.5×3.5 cm^2, matrix size of 256×256 and a spatial resolution of 0.137 mm) was used for T_1 relaxation time measurements. Scans were continuously used before and after contrast agent injection for up to 120 min. Two transverse slices which encompassed the biggest area of the tumour were chosen. From the T_1-weighted images, specific regions of interest (ROIs) were chosen according to the combined views of the signal intensity changes in the difference images and T_2-weighted images. Four groups of ROIs were chosen as follows: tumour periphery (PT), periphery region around necrotic area (PN), tumour interior (TI) with a minimal signal intensity change and not associated with a necrotic area and normal brain tissue (N) found on the contralateral side. Following mMRI, rats were killed and brains were extracted and fixed for fluorescence staining. For each type of ROIs specified above (PT, PN, TI or N), three specific ROIs (defined circles), based on altered signal intensities, were analysed from each animal ($n = 3$ for either VEGFR2 probe or IgG contrast agent administered rats). Regional signal intensities were therefore calculated from nine values for each type of ROIs. A contrast difference image was created from the pre- and post-contrast datasets for the slice of interest, by computing the difference in signal intensity between the post-contrast and the pre-contrast image on a pixel basis.

MRA was obtained by using a FLASH (fast low angle shot) method with a TR of 25 msec. and a TE of 2.3 msec., a flip angle of 25°, in a volume of interest in the rat brain region of $2.6 \times 1.7 \times 1.1$ cm3 placed at an angle of 5° relative to the horizontal plane. As previously described by our group [15], we used a Mathematica (6.0) based program to quantify cerebral blood volumes. Briefly, a voxel of interest which includes the branches of the middle cerebral artery supplying the frontal cortex was chosen, and the high-intensity pixels due to flowing blood (choosing a constant intensity threshold for all datasets), were analysed to measure the total blood volume in the specified ROI. Four rats were used for tumour volume calculations and cerebral blood volumes at 7, 14, 18 and 24 days following C6 cell intracerebral implantations. Following the last MRI session, the rats were killed (CO_2 inhalation), and brain tissues were fixed for immunohistochemistry to assess VEGFR2 levels. The MRA dataset was zero-filled to provide a $512 \times 512 \times 256$ matrix and is displayed as a 2D transverse projection (grey pixels) co-registered on a T_2-weighted image showing the glioma. For co-registration, translations and scaling factors are calculated from the difference in field of view and in position of the magnet isocentre of both datasets (information provided by the 'method' file generated by Paravision software during MRI acquisition) by using Mathematica-based program. The datasets are then implemented in the data visualization software Amira 4.1.0 (Mercury Computer Systems, Chelmsford, MA, USA) to provide a visualization of the co-registration for the two datasets. Three-dimensional visualization of the tumour, provided by interpolating the glioma ROIs between slices by using Amira, was co-registered with the 3D vasculature dataset. The glioma is represented as a 'SurfaceView', and the angiogram as an 'Isosurface' with an intensity threshold of 12,500. The overlay of the contrast difference image and the 3D brain vasculature was generated using Amira, representing the difference image as an 'Orthoslice', and the angiogram as an 'Isosurface' with an intensity threshold of 12,500.

Calculations of relative probe concentration

Relative probe (contrast agents) concentrations, C (units: M), were calculated for the selected ROI using the following formula [23]: $C \propto [1/T_1 \text{ (after)} - 1/T_1 \text{ (before)}]$, where $1/T_1$ (after) is the T_1 rates taken at different time-points after injection of probe, $1/T_1$ (before) is the T_1 rates taken before injection of probe. The T_1 value of a specified ROI was computed from all the pixels in the ROI by the following equation [23] (processed by ParaVision 4.0, Bruker): $S(\text{TR}) = S_0(1 - e^{-\text{TR}/T1})$, where TR is the repetition time (units: msec.), S_0 is the signal intensity (integer machine units) at TR $>>$ T_1 and TE $= 0$, and T_1 is the constant of the longitudinal relaxation time (units: msec.).

Fluorescence staining

After the 2 hrs mMRI protocol, the brains from four rats (two injected with VEGFR2 probe and another two injected with control-IgG contrast agent) were extracted, the tumour side (PT) and contralateral side of the brain were cut and fixed in Z-fixative (zinc formalin: formaldehyde 3.7%, zinc sulphate). The tissue was then washed with PBS and incubated with 15% sucrose before embedding in optimal cutting temperature compound and freezing in liquid nitrogen. The cryosections were then stained with Cy3-labelled streptavidin, which can bind to the biotin moiety of the albumin-Gd-DTPA-biotin contrast agent within the brain tissue.

Another rat injected with the VEGFR2 probe was anesthetized and cardiac perfused with PBS and 4% paraformaldehyde. The whole brain was extracted and fixed in 4% paraformaldehyde. After scanning of the whole brain, the brain sections which represented the exact location from PT, PN, TI and N regions were chosen, sliced and stained for multiple staining. For localization of the VEGFR2 probe and correlation with endothelial cells, the brain sections were stained with Cy3-labelled streptavidin for the VEGFR2 probe, and rabbit anti-laminin followed by donkey anti-rabbit Alexa 488 for the laminin-containing endothelial basement membrane. The nucleus was stained with 4′,6-diamidino-2′-phenylindole (DAPI) (blue). For comparison of VEGFR2 probe localization, VEGFR2 tissue levels and vascularization, the brain sections were stained with Cy3-labelled streptavidin for the VEGFR2 probe, rabbit anti-laminin/donkey-anti-rabbit Alexa 488 and rabbit anti-VEGFR2/Cy5- labelled donkey-anti-rabbit antibodies for the total cellular VEGFR2 expression levels. Alexa fluor-647 anti-rat CD45 mouse IgG was used for fluorescence staining of CD45.

Stained tissue slices were examined with a Nikon C1 confocal laser scanning microscope (Nikon Instruments, Melville, NY, USA). Image collection parameters (neutral density filters, pinhole and detector gains) were kept constant during image acquisition, to make reliable comparisons between specimens. The measurement of fluorescence intensity was done as described [24]. In brief, five images were collected for each experimental condition, and the mean fluorescence intensity of 15–20 ROIs per image was integrated using the EZ-C1 software (Nikon). Co-localization analysis was done using a Imaris Coloc module (Imaris vs. 6.4), and data were presented as percentage co-localization and the Manders co-localization coefficient [25].

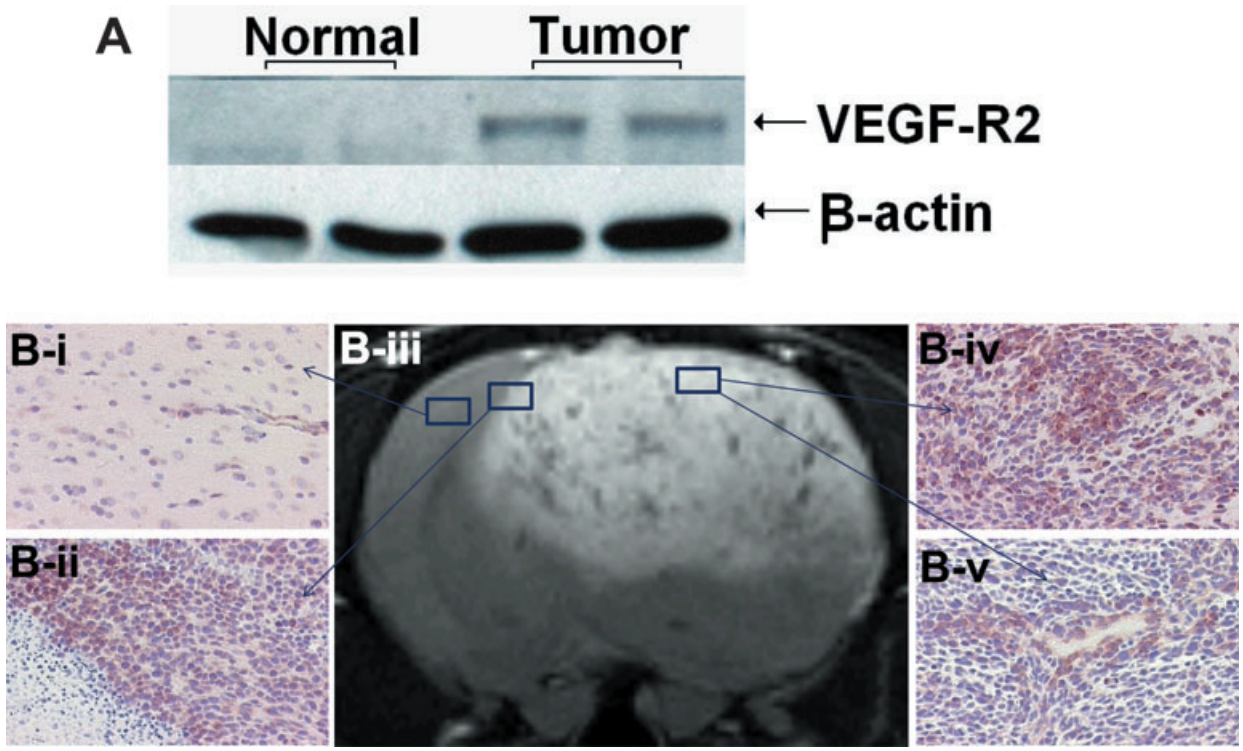

Fig. 1 VEGFR2 overexpression in C6 rat gliomas. (**A**) Western blotting of VEGFR2 from normal brain and C6 gliomas. β-actin is used as loading control. (**B**) Immunohistochemical localizations of VEGFR2 (20× magnification) in normal brain tissue (**B**-i), tumour boundary (**B**-ii) and PT (**B**-iv) shows glioma cells; (**B**-v) shows cross-section of a vessel). Representative T_2-weighted image (**B**-iii) was taken at day 24.

Statistical analyses

For the molecular MRI datasets, statistical analyses was done using a Student's two-tailed t-test, between either the anti-VEGFR2 probe and IgG contrast agent administered animals, brain tissue ROIs in 'normal' contralateral (N) and glioma PT, peri-necrotic (PN) and interior (TI), tumour blood volume *versus* time, or VEGFR2 probe concentration *versus* either tumour or tumour blood volumes. A *P*-value <0.0001, <0.001, <0.01 or <0.05 was considered statistically significant. Data are represented as mean ± S.D. For the mean fluorescence analysis, data were statistically analysed using one-way ANOVA with a Bonferroni's multiple comparison test. Statistical significance was obtained between tissues when a *P*-value <0.01.

Results

In vitro assessment of VEGFR2 expression by Western blotting and immunohistochemistry

Figure 1A shows an enhanced VEGFR2 expression in C6 gliomas, compared to no band for VEGFR2 expression in normal brain by Western blotting. In the immunohistochemistry staining for VEGFR2 in C6 gliomas and contralateral normal brain, VEGFR2 is strongly expressed in microvessels among dense glioma cells (Fig.1B-iv), and also on the endothelial cells lining around the big blood vessels (Fig. 1B-v).

In vivo detection and quantification of VEGFR2 expression

As illustrated by Fig. 2, the molecular targeting probe that we used in this study is an anti- VEGFR2 mAb linked to the albumin moiety of biotinylated albumin-(Gd-DTPA). A series of T_1-weighted images were taken before and at various time-points after administration of the Gd-based probe to assess the location of binding of the probe to VEGFR2. A difference image (Fig. 3A, B-iii) was obtained which was the subtraction between the T_1 images of pre- (Fig. 3A, B-i) and 2 hrs after (Fig. 3A, B-ii) injection of the contrast agent. In the rats injected with the control-IgG contrast agent, there was not much difference after injection up to 2 hrs in the tumour region as showed in Fig. 3A-iii (data not shown for time-points prior to 2 hrs). This indicates that almost none or very little of the control probe was taken up by the tumour tissue, or remained after 2 hrs. However, significant changes occurred in the rats injected with anti-VEGFR2 probe. Figure 3B-ii shows a

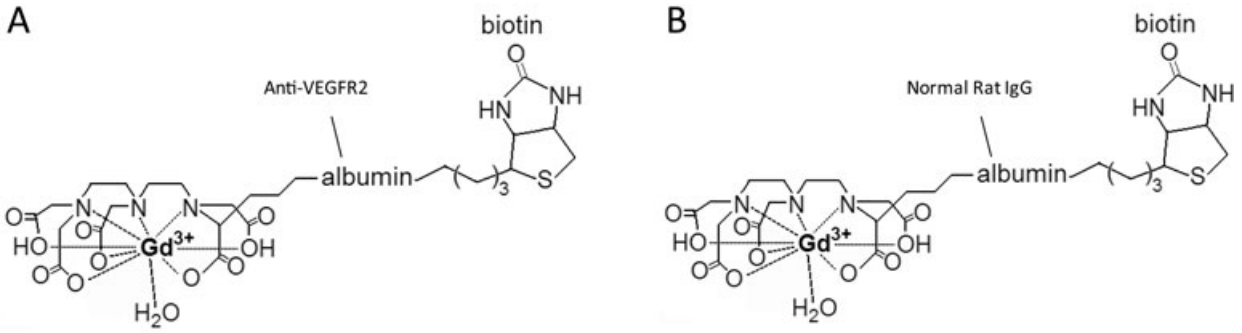

Fig. 2 Structures of the biotinyl-albumin-Gd-DTPA based targeting agents. Specific anti-VEGFR2 mAb conjugated to the albumin moiety in the contrast agent (**A**), and normal rat IgG- conjugated contrast agent (**B**).

dramatic increase in MR signal intensity in parts of the tumour region 2 hrs after injection, and this change was clearly depicted in the difference image (Fig. 3B-iii). Strong anti-VEGFR2 probe uptake indicates strong VEGFR2 expression in the tumour regions. Figure 3A, B-iv shows a corresponding T_2-weighted image taken before the injection. Using a combination of both difference images and T_2-weighted images, we defined four groups of ROIs as PT, PN, TI and N. The necrotic area was depicted as a dark region in T_2 images with little uptake of the anti-VEGFR2 probe as shown in a difference image.

For the regions where the probe was bound, there were different increases in signal intensities in different glioma region. Two hours following injection of the VEGFR2 probe, PT and PN regions had the most significant MR signal intensity increases (12-fold for PT and 10-fold for PN, compared to the contralateral brain tissue, whereas the TI region was only 2.3-fold compared to the contralateral region; Fig. 4A). There were minimal changes in signal intensity in either all brain regions in the control-IgG injected rats, or within the contralateral brain tissue in the VEGFR2 targeted rats. The signal intensities changed dynamically during 2 hrs' MRI observation. For instance, signal intensity in the PT region kept increasing significantly from 20 min. after injection of the VEGFR2 probe, compared to the PT region in control-IgG injected rats (Fig. 4B).

Fluorescence staining at 2 hrs after administration of the probe confirmed that the distribution of VEGFR2 probe was higher in the tumour region. In all fluorescence images the VEGFR2 probe was stained red with streptavidin-Cy3, which bound to the biotin moiety of the probe. Figure 5 showed a high intensity for the VEGFR2 probe in the tumour region (obtained from the glioma periphery region) (Fig. 5D), and the mean fluorescence intensity of probe in the tumour region was found to be significantly higher than that measured in contralateral brain tissue or glioma tissue from a control-IgG injected rat (Fig. 5F).

The differentiation of VEGFR2 expression in different glioma regions was confirmed in Fig. 6B. The probe was seen to be distributed mainly in PT and PN regions (Fig. 6B-ii and iv), whereas the TI (not associated with necrosis) was found to have less probe levels. The total cellular VEGFR2 expression was also assessed at 2 hrs in the peripheral regions of gliomas. Co-localization of VEGFR2 levels (blue) and probe (red) are indicated by the presence of white (Fig. 6C-v and vi), where the co-localization percentage was 50.66% (with a thresholded Mander's coefficient of 0.4607) for cellular VEGFR2 (blue) and VEGFR2 probe (red), and 46.87% (with a thresholded Mander's coefficient of 0.4342) for co-localization of the VEGFR2 probe (red) and laminin (green), a marker for endothelial cells. Furthermore, the fluorescence staining of CD45, a common antigen found on leucocytes, showed that the VEGFR2 probe (red) was poorly co-localized with CD45 (blue) (Fig. 6D-i–iii), indicating that the distribution of the VEGFR2 probe was not associated with infiltrated leucocytes in the glioma tissue.

Visualization of vasculature associated with VEGFR2 expression and changes of CBV

The blood of the frontal cortex, where the tumour is located, is supplied by the middle cerebral artery. A representative 2D MR angiogram was overlaid onto a T_2-weighted tumour morphological MR image (Fig. 7A). The regional blood volume in the rectangular region, which encompassed blood vessels that supplied the tumour, was calculated and found to increase correspondingly with an increase in tumour volumes (Fig. 7C). As shown in Fig. 7B, three-dimensional vasculature was co-registered with a 3D tumour, which further illustrated the morphology and position of tumour vasculature. VEGFR2 expression, as indicated by the probe concentration, was found to be ideally correlated with tumour and tumour blood volumes ($R^2 = 0.97$ and $R^2 = 0.99$, respectively) (Fig. 7D). There is a direct relationship with an increase in VEGFR2 probe concentration (from chosen ROIs) as tumour or tumour blood volumes increase. Figure 7E shows the co-registration of the 3D vasculature with VEGFR2 expression (as shown in the MR contrast difference image, and also shown in Fig. 3B-iii) image. The high-VEGFR2 expression regions (shown as high signal intensities) in the tumour observed by mMRI, have an enhanced blood supply (Fig. 7E) from the middle cerebral artery (particularly in the PT regions) as observed by MRA, compared to that in contralateral brain.

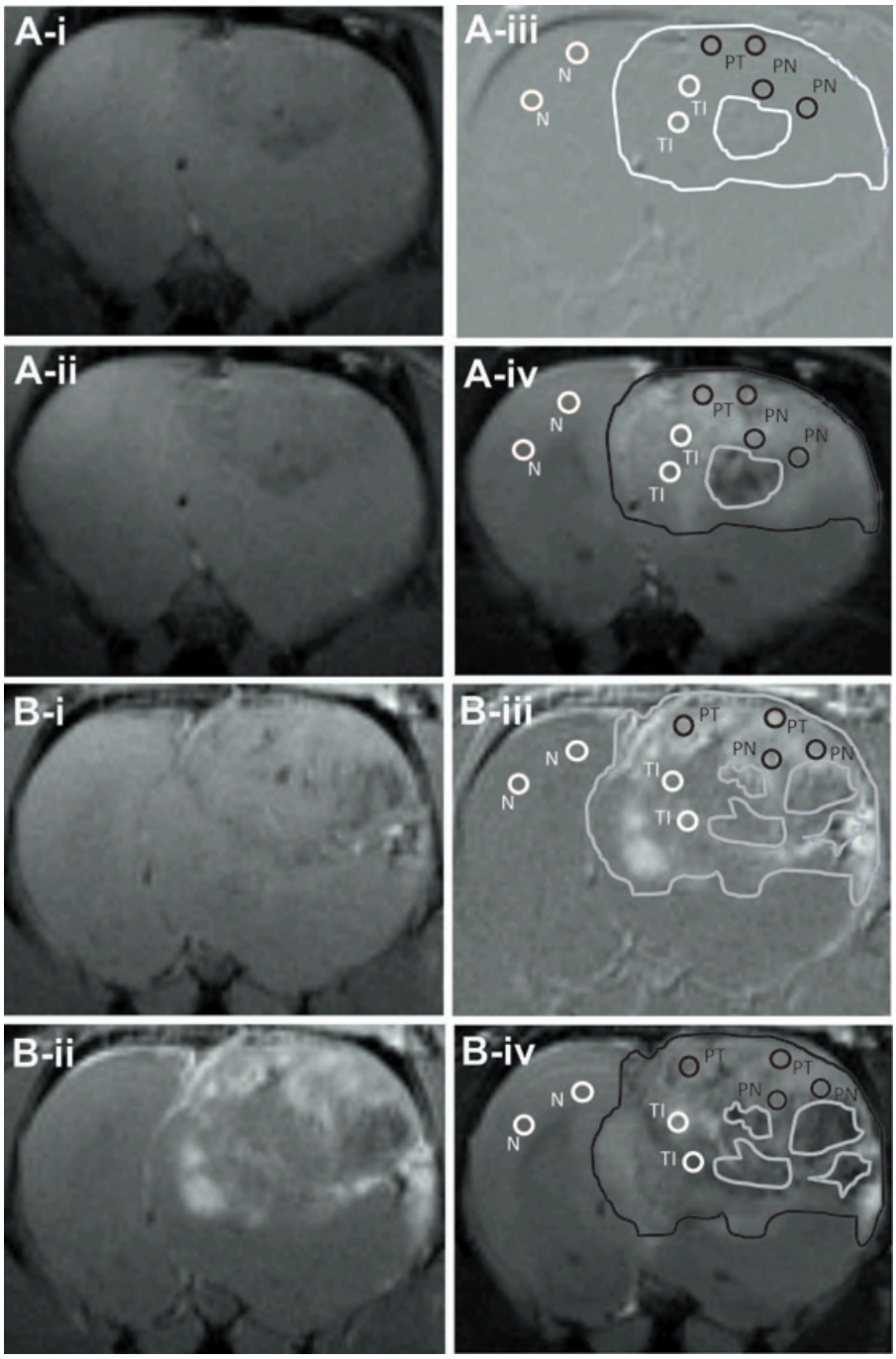

Fig. 3 T_1 weighted MR images obtained before and 2 hrs after injection of control IgG (**A**-i and -ii) and VEGFR2-mAb (**B**-i and -ii) -linked mMRI agents, with corresponding difference images (iii) and T_2-weighted images obtained before injection of the contrast agent (iv). Representatives of ROIs in each group are depicted as circles, using for calculating signal intensities and probe concentrations in Figure 4. The edges of the tumours were also lined out, as well as the necrotic areas inside the tumours. Contralateral normal tissue is labelled as N, tumour periphery as PT, periphery around the necrotic area as PN, and tumour interior with less positive signal as TI.

Discussion

Non-invasive mMRI is a key component of molecular imaging which developed mainly over the last decade [26]. Using mMRI to monitor tumour angiogenesis is beneficial in the early diagnosis, and accurate grading of a tumour, and for the development of anti-angiogenic drug therapy [27, 28]. VEGF/VEGFR has been well demonstrated as a critical signalling pathway in the development of tumour angiogenesis [29, 30]. Mainly two high-affinity receptors for VEGF are involved in angiogenesis, VEGFR1 (flt-1), which is a negative regulator, whereas VEGFR2 (flk-1) is a positive regulator. Millauer *et al.* have demonstrated that

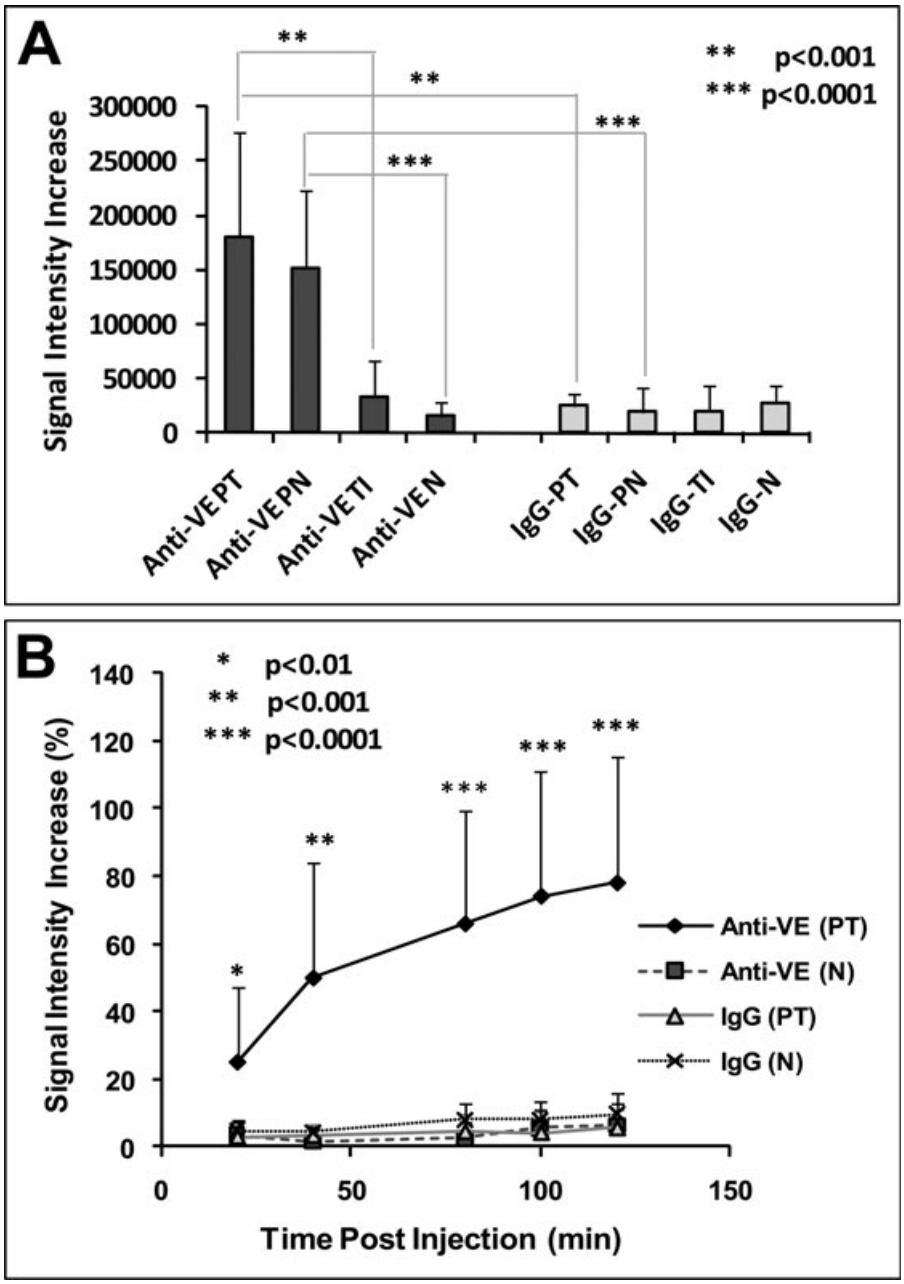

Fig. 4 (**A**) Differences in signal intensities changes in ROIs depicted in Fig. 3. Signal intensity increases are measured between 2 hrs after and before administration of control-IgG or VEGFR2-mAb linked mMRI agents. (**B**) Dynamic changes of signal intensity increase percentages in PT and N area after injection of the contrast agents (significance is made by PT area between VEGFR2-mAb and control-IgG group). Three ROIs were calculated in each particular region (PT, PN, TI and N). The data were shown as mean ± S.D. Significant differences were obtained (using a Student's t-test) if $*P < 0.01$, $**P < 0.001$ or $***P < 0.0001$.

expression of dominant-negative flk-1 reduced neovascularization prolonged the survival time after implantation of C6-derived gliomas [31]. As demonstrated by Western blotting and immunohistochemistry for the detection of VEGFR2 in our study, we confirmed that VEGFR2 is overexpressed in rat gliomas. However, the accurate detection of VEGF/VEGFR2 could be a crucial marker for the diagnosis of angiogenesis. The fact that VEGF is soluble and dynamic makes imaging of VEGF more challenging [26]. Therefore, the extracellular marker VEGFR2 which is expressed mainly on angiogenic endothelial cells is an ideal target for imaging by mMRI.

In the current study, we used an anti-VEGFR2 mAb linked to a Gd-based contrast agent to target VEGFR2 on endothelial cells induced by C6 gliomas. Gd is a paramagnetic transition metal which can induce a great T_1 effect on surrounding water molecules. Gd-based dynamic contrast enhanced MRI has been increasingly employed to study angiogenesis in tumours, and the early response to angiogenic therapy [32–34]. Our study demonstrated

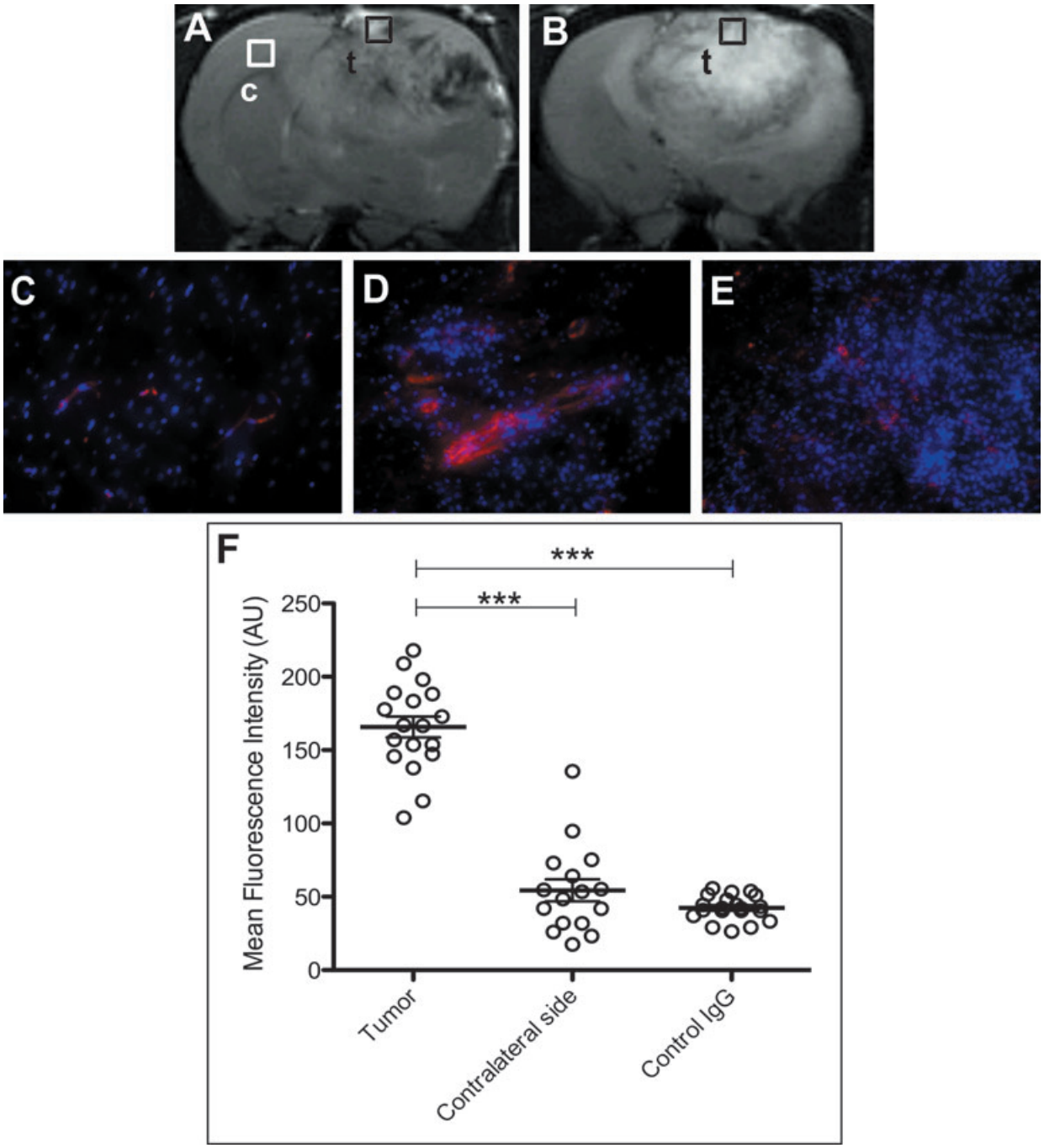

Fig. 5 (**A**) and (**B**) are the representative T_2-weighted images from rats injected with the VEGFR2 probe or the control-IgG contrast agent, respectively. Fluorescence detection of the probe was made in either contralateral brain (**C**), or glioma tissue (**D**) at 2 hrs following administration of the VEGFR2 probe, or in glioma tissue (**E**) at 2 hrs after administration of the control-IgG contrast agent. The tissue locations are indicated by square boxes, 'c' for contralateral brain and 't' for tumour. The biotin groups from the contrast agents were stained with Cy3-labelled streptavidin (red fluorescence), and nuclei were stained with DAPI (blue fluorescence; 20× magnification). (**F**) Mean fluorescence intensities for the VEGFR2 probe injected in rats in the tumour region (as in **D**), for VEGFR2 probe injected rats in contralateral brain tissue (as in **C**), or for control IgG injected rats in the tumour region (as in E). $***P < 0.01$ indicates significance between (**D**) and (**C**), or between (**D**) and (**E**). Statistics were done using ANOVA with a Bonferroni's multiple comparison test.

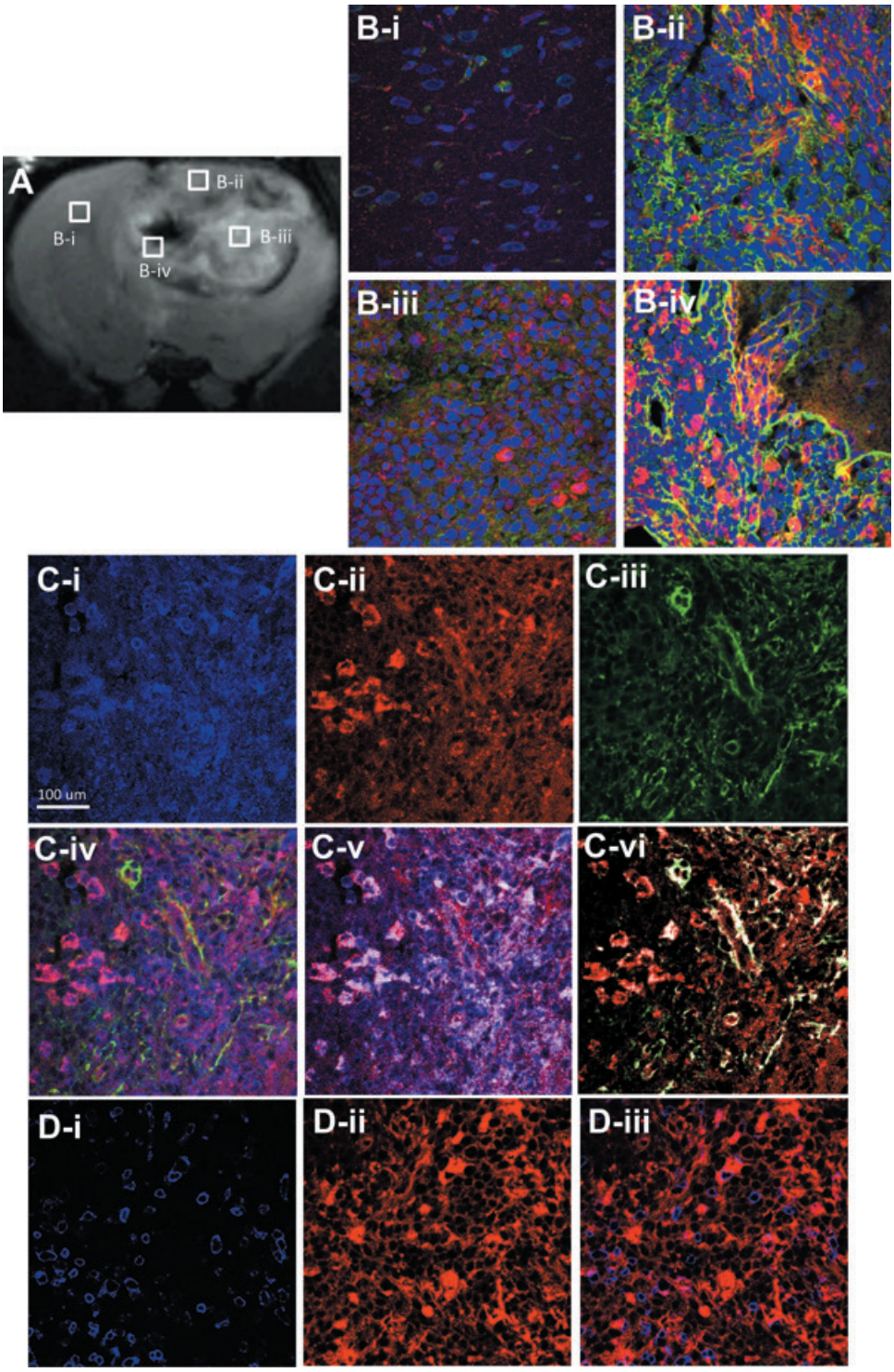

Fig. 6 Confirmation of distribution and localization of VEGFR2 probe targeting by fluorescence staining. Fluorescence staining of VEGFR2 probe (red) and laminin (green) in N (**B**-i), PT (**B**-ii), TI (**B**-iii) and PN (**B**-iv) 2 hrs after injection of VEGFR2 probe. Nuclei were stained with DAPI (blue). (**A**) T_2-weighted image showing the morphology of tumour and location of the ROIs. (**C**-i–vi) Fluorescence staining of the probe (red), cellular VEGFR2 (blue) and laminin (green) in PT region. (**C**-iv) Co-localization of the probe, cellular VEGFR2 and laminin. (**C**-v) Thresholded co-localization of the probe and cellular VEGFR2. (**C**-vi) Thresholded co-localization of the probe and laminin. (**D**-i–iii) Dual-fluorescence labelling for the VEGFR2 probe (red) and CD45 (blue), a marker for leucocytes, in the PT region. Magnification ×60.

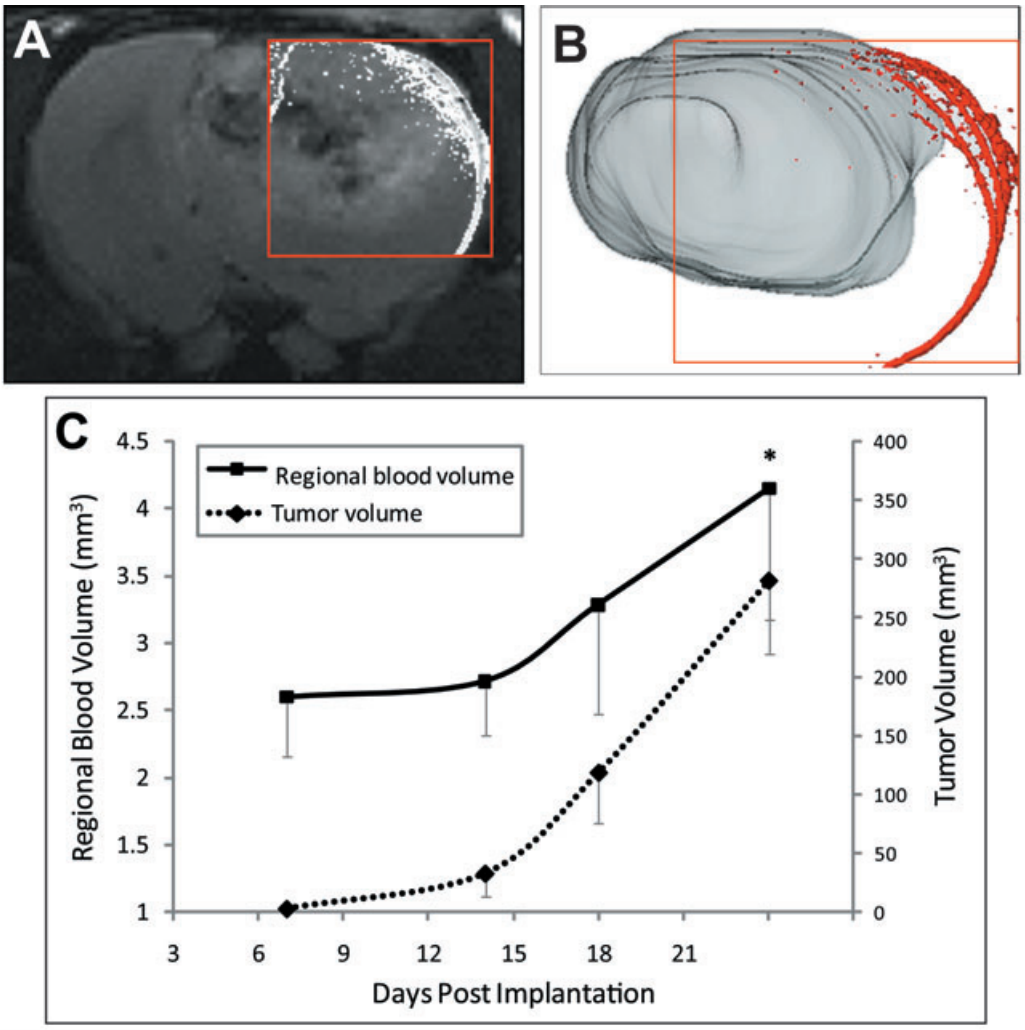

Fig. 7 (**A**) A representative tumour vascular MR angiogram overlaid with a T_2-weighted MR image (transverse orientation) of a C6 glioma. (**B**) 3D vasculature image (obtained from MRA) superimposed on a 3D rendered image of a C6 glioma (using Amira). (**C**) Increases in tumour blood volume with corresponding increases in tumour volume during the tumour growth time course. The data are represented as the mean ± S.D. $*P < 0.05$, by a Student's t-test, indicates a significant difference between days 24 and 7. (**D**) Increases in VEGFR2 expression is related with increases in tumour and tumour blood volumes. VEGFR2 expression is indicated by VEGFR2 probe concentration which was calculated as differences in T_1 rates from 2 hrs after injection of the probe and pre-injection datasets. $*P < 0.01$ and $***P < 0.0001$ (Student's t-test) indicates significance differences in VEGFR2 levels between rats (three ROIs from each) which have the most and the least tumour volumes, and between those which have the middle and the least tumour volumes, respectively. R^2 indicates the linear relationship between VEGFR2 probe concentration and either tumour volume, or tumour blood volume. (**E**) Reconstructed MR angiography data of the middle cerebral arteries in the tumour region (right) and contralateral brain tissue (left) was superimposed on a difference MR image (obtained from T_1-weighted images between 2 hrs after injection and before injection of the VEGFR2 probe; also shown in Fig. 3B-iii).

differentiation in VEGFR2 levels within various tumour regions. The high levels of VEGFR2 in PT and PN regions indicated an active neovascularization event occurring in PT and PN during glioma development. C6 gliomas tend to form foci of necrosis within the tumour [35]. The low-signal areas which were depicted by T_2-weighted images, and found to be necrotic areas by histology, had almost no expression of VEGFR2 (Fig. 3B) in VEGFR2 targeted rats. In the TI, there is a region between PT and PN, showing minimal probe concentration, which suggested a limited vascularization in this specific region. The non-specific binding of the control IgG contrast agent in the tumour tissue was minimal which suggested the quick 'wash-out' of the contrast agent after it leaked through the tumour vasculature without specifically binding to the tissue. The different levels of VEGFR2 established the heterogeneous nature of angiogenesis within tumours where the periphery of tumour had the most abundant neovasculature. The ability to detect various degrees of VEGFR2 expression in the tumour region indicated the high specificity of the Gd-based VEGFR2-mAb probe and high sensitivity of the mMRI method. In addition, this study also allowed us to observe the dynamic process of how the targeted probe interacted with the microvessels in the brain tissue, as shown by signal intensity changes in different regions over time.

The high levels of the VEGFR2 probe in the glioma periphery regions, 2 hrs after injection, was confirmed by the mean fluorescence measurements obtained from fluorescence images following staining of the biotin moiety on the probe in the tissues with Cy3-labelled streptavidin. The fluorescence imaging data showed a relatively high co-localization of the VEGFR2 probe with cellular VEGFR2, as well as the endothelial cell marker laminin. Laminin is a major component of the endothelial basement membrane, and thus is a reliable marker of the vascular endothelium [36]. These results demonstrated that the VEGFR2 probe, abundant in PT and PN areas, was found to target the VEGFR2 expressed on endothelial cells that were also marked by laminin, as demonstrated by the co-localization between the probe, cellular VEGFR2 and laminin. It has been demonstrated by Dineen *et al.* that tumour-associated macrophages, which infiltrate into pancreatic tumours, have been found to express VEGFR2 [37]. In order to determine if the VEGFR2 probe is targeting any VEGFR2 expressed by infiltrating leucocytes, dual fluorescence staining for CD45, a common leucocyte antigen, and the presence of the probe, was done. The poor co-localization between CD45 and the probe indicated that the VEGFR2 probe mainly targeted VEGFR2 expressed on vascular endothelial cells in glioma tissue, and not infiltrating leucocytes.

In this study, we used MRA to visualize angiogenesis in a C6 tumour. Two- or three-dimensional vasculature images superimposed on tumour morphological images provide excellent visualization of the tumour and its associated blood supply. Quantification of tumour blood volumes was used to further confirm the presence of angiogenesis that corresponded with tumour growth. Co-registration of 3D vasculature with a molecular MR difference image illustrated that the VEGFR2 high-expression regions had increased blood supply, particularly in the peripheral regions of the tumour. Varying tumour volumes that were targeted with the VEGFR2 probe, allowed us to study the correlation of VEGFR2 probe levels with tumour and tumour blood volumes. Our data indicated that the level of VEGFR2 expression increased as tumour and tumour blood volumes (an indication of angiogenesis) both increased. This could be another dynamic index to evaluate angiogenesis, in addition to the differentiation of VEGFR2 expression in different tumour regions.

To our understanding, we are the first group to directly investigate *in vivo* VEGFR2 expression with a Gd-based probe specific for VEGFR2 in a C6 glioma model by using mMRI. Although PET is still the most widely used in all of the imaging modalities for VEGF/VEGFR2 [26, 38], mMRI has a great advantage as a non-radionuclide-based imaging modality. With the use of a high magnetic field (7 Tesla) and a highly specific mAb which is bound to the albumin-Gd based contrast agent, our study overcame the major disadvantage of mMRI for its inherent low sensitivity [26] and successfully monitored the heterogeneous expression of VEGFR2 in different tumour regions. Albumin-(Gd-DTPA) has been very useful in characterizing microvessels in tumours, though it is not yet being commercially developed. Mazola *et al.* utilized this contrast agent for measuring trans-endothelial permeability and fractional plasma volume which showed to be correlated with microvessel density by immunostaining for CD31, and they also detected the effect of SU6668 [an inhibitor of VEGFR2, platelet-derived growth factor-β and fibroblast growth factor receptor (FGFR)] which decreased angiogenesis in a mouse colon carcinoma model [39]. Our study confirmed the ability of Albumin-(Gd-DTPA) to carry a specific antibody for binding to an extracellular antigen associated with tumour blood vessel functionally. An extension of this study would be to assess *in vivo* VEGFR2 levels in different rodent glioma models varying in tumour aggressiveness or grades. Our study may also be of

interest for using this method to target VEGFR2 to assess anti-angiogenic therapy.

Acknowledgements

We thank the Oklahoma Medical Research Foundation, the Oklahoma Center for the Advancement of Sciences and Technology (grant AR052–132), and the National Institutes of Health (National Cancer Institute grant 5R03CA121359–2), for their funding assistance.

Conflict of interest

The authors confirm that there are no conflicts of interest.

References

1. **Folkman J.** New perspectives in clinical oncology from angiogenesis research. *Eur J Cancer*. 1996; 32A: 2534–9.
2. **Vidal S, Kovacs K, Lloyd RV, *et al*.** Angiogenesis in patients with craniopharyngiomas: correlation with treatment and outcome. *Cancer*. 2002; 94: 738–45.
3. **Korkolopoulou P, Patsouris E, Kavantzas N, *et al*.** Prognostic implications of microvessel morphometry in diffuse astrocytic neoplasms. *Neuropathol Appl Neurobiol*. 2002; 28: 57–66.
4. **Leung DW, Cachianes G, Kuang WJ, *et al*.** Vascular endothelial growth factor is a secreted angiogenic mitogen. *Science*. 1989; 246: 1306–9.
5. **Hiratsuka S, Kataoka Y, Nakao K, *et al*.** Vascular endothelial growth factor A (VEGF-A) is involved in guidance of VEGF receptor-positive cells to the anterior portion of early embryos. *Mol Cell Biol*. 2005; 25: 355–63.
6. **Plate KH, Breier G, Weich HA, *et al*.** Vascular endothelial growth factor and glioma angiogenesis: coordinate induction of VEGF receptors, distribution of VEGF protein and possible *in vivo* regulatory mechanisms. *Int J Cancer*. 1994; 59: 520–9.
7. **Motzer RJ, Michaelson MD, Redman BG, *et al*.** Activity of SU11248, a multitargeted inhibitor of vascular endothelial growth factor receptor and platelet-derived growth factor receptor, in patients with metastatic renal cell carcinoma. *J Clin Oncol*. 2006; 24: 16–24.
8. **de Bouard S, Herlin P, Christensen JG, *et al*.** Antiangiogenic and anti-invasive effects of sunitinib on experimental human glioblastoma. *Neuro Oncol*. 2007; 9: 412–23.
9. **Lindner V, Reidy MA.** Expression of VEGF receptors in arteries after endothelial injury and lack of increased endothelial regrowth in response to VEGF. *Arterioscler Thromb Vasc Biol*. 1996; 16: 1399–405.
10. **Plate KH, Risau W.** Angiogenesis in malignant gliomas. *Glia*. 1995; 15: 339–47.
11. **Kang HW, Josephson L, Petrovsky A, *et al*.** Magnetic resonance imaging of inducible E-selectin expression in human endothelial cell culture. *Bioconjug Chem*. 2002; 13: 122–7.
12. **Kang HW, Torres D, Wald L, *et al*.** Targeted imaging of human endothelial-specific marker in a model of adoptive cell transfer. *Lab Invest*. 2006; 86: 599–609.
13. **Winter PM, Caruthers SD, Kassner A, *et al*.** Molecular imaging of angiogenesis in nascent Vx-2 rabbit tumors using a novel alpha(nu)beta3-targeted nanoparticle and 1.5 tesla magnetic resonance imaging. *Cancer Res*. 2003; 63: 5838–43.
14. **Backer MV, Gaynutdinov TI, Patel V, *et al*.** Vascular endothelial growth factor selectively targets boronated dendrimers to tumor vasculature. *Mol Cancer Ther*. 2005; 4: 1423–9.
15. **Doblas S, Saunders D, Kshirsagar P, *et al*.** Phenyl-tert-butylnitrone induces tumor regression and decreases angiogenesis in a C6 rat glioma model. *Free Radic Biol Med*. 2008; 44: 63–72.
16. **Towner RA, Smith N, Doblas S, *et al*.** *In vivo* detection of c-Met expression in a rat C6 glioma model. *J Cell Mol Med*. 2008; 12: 174–86.
17. **Towner RA, Smith N, Tesiram YA, *et al*.** *In vivo* detection of c-MET expression in a rat hepatocarcinogenesis model using molecularly targeted magnetic resonance imaging. *Mol Imaging*. 2007; 6: 18–29.
18. **Schmiedl U, Brasch RC, Ogan MD, *et al*.** Albumin labeled with Gd-DTPA. An intravascular contrast-enhancing agent for magnetic resonance blood pool and perfusion imaging. *Acta Radiol Suppl*. 1990; 374: 99–102.
19. **Kobayashi N, Allen N, Clendenon NR, *et al*.** An improved rat brain-tumor model. *J Neurosurg*. 1980; 53: 808–15.
20. **Benda P, Lightbody J, Sato G, *et al*.** Differentiated rat glial cell strain in tissue culture. *Science*. 1968; 161: 370–1.
21. **Dafni H, Landsman L, Schechter B, *et al*.** MRI and fluorescence microscopy of the acute vascular response to VEGF165: vasodilation, hyper-permeability and lymphatic uptake, followed by rapid inactivation of the growth factor. *NMR Biomed*. 2002; 15: 120–31.
22. **Hermanson GT.** Bioconjugate techniques. New York: Academic Press; 1996.
23. **E. Mark Haacke RWB, Michael R. Thompson.** Magnetic resonance imaging: physical principles and sequence design. New York: Wiley-Liss; 1999.
24. **Lupu C, Westmuckett AD, Peer G, *et al*.** Tissue factor-dependent coagulation is preferentially up-regulated within arterial branching areas in a baboon model of Escherichia coli sepsis. *Am J Pathol*. 2005; 167: 1161–72.
25. **E. M. M. Manders FJVJAA.** Measurement of co-localization of objects in dual-colour confocal images. *J Microsc*. 1993; 169: 375–82.
26. **Cai W, Chen X.** Multimodality molecular imaging of tumor angiogenesis. *J Nucl Med*. 2008; 49: 113–28S.
27. **Cai W, Rao J, Gambhir SS, *et al*.** How molecular imaging is speeding up antiangiogenic drug development. *Mol Cancer Ther*. 2006; 5: 2624–33.
28. **Iagaru A, Chen X, Gambhir SS.** Molecular imaging can accelerate anti-angiogenic drug development and testing. *Nat Clin Pract Oncol*. 2007; 4: 556–7.
29. **Cai W, Chen X.** Multimodality imaging of vascular endothelial growth factor and vascular endothelial growth factor receptor expression. *Front Biosci*. 2007; 12: 4267–79.
30. **Ferrara N.** The role of VEGF in the regulation of physiological and pathological angiogenesis. *EXS*. 2005; 94: 209–31.
31. **Millauer B, Shawver LK, Plate KH, *et al*.** Glioblastoma growth inhibited *in vivo* by a

dominant-negative Flk-1 mutant. *Nature*. 1994; 367: 576–9.

32. **Padhani AR, Husband JE.** Dynamic contrast-enhanced MRI studies in oncology with an emphasis on quantification, validation and human studies. *Clin Radiol*. 2001; 56: 607–20.
33. **Runge VM.** Safety of approved MR contrast media for intravenous injection. *J Magn Reson Imaging*. 2000; 12: 205–13.
34. **Tofts PS, Brix G, Buckley DL, *et al*.** Estimating kinetic parameters from dynamic contrast-enhanced T(1)-weighted MRI of a diffusable tracer: standardized quantities and symbols. *J Magn Reson Imaging*. 1999; 10: 223–32.
35. **Grobben B, De Deyn PP, Slegers H.** Rat C6 glioma as experimental model system for the study of glioblastoma growth and invasion. *Cell Tissue Res*. 2002; 310: 257–70.
36. **Beck K, Hunter I, Engel J.** Structure and function of laminin: anatomy of a multidomain glycoprotein. *FASEB J*. 1990; 4: 148–60.
37. **Dineen SP, Lynn KD, Holloway SE, *et al*.** Vascular endothelial growth factor receptor 2 mediates macrophage infiltration into orthotopic pancreatic tumors in mice. *Cancer Res*. 2008; 68: 4340–6.
38. **Cai W, Chen K, Mohamedali KA, *et al*.** PET of vascular endothelial growth factor receptor expression. *J Nucl Med*. 2006; 47: 2048–56.
39. **Marzola P, Degrassi A, Calderan L, *et al*.** *In vivo* assessment of antiangiogenic activity of SU6668 in an experimental colon carcinoma model. *Clin Cancer Res*. 2004; 10: 739–50.